www.ietdl.org

Published in IET Microwaves, Antennas & Propagation
Received on 16th June 2010
Revised on 12th January 2011
doi: 10.1049/iet-map.2010.0251

ISSN 1751-8725

Wideband antenna array beam steering with free-space optical true-time delay engine

N.K. Nahar B. Raines R.G. Rojas B. Strojny

ElectroScience Laboratory, Department of Electrical and Computer Engineering, The Ohio State University, 1320 Kinnear Road, Columbus, OH 43212, USA
E-mail: nahar.2@osu.edu

Abstract: A 6–12 GHz Vivaldi wideband antenna array made of four sub-arrays (two elements per sub-array) was built to steer the beam with a White cell optical true-time delay (OTTD) engine. The OTTD engine was simulated to produce delays with a time delay increment of 25 ps. The beam is then steered combining the simulated OTTD delays and the measured mutual coupling of a Vivaldi array to a maximum scan angle of $\pm 50^{\circ}$. The results demonstrate that the effect of optical losses and mutual coupling effects of the combined beam steering system is not negligible and must be carefully accounted for when implementing frequency-independent TTD beam steering systems.

1 Introduction

Beam steering with optical true time delay (OTTD) has been demonstrated successfully with fibre optics [1, 2] and waveguides [3]. Among free-space OTTD systems, White cell TTD engines have enormous potential for beam steering owing to their lower loss (compared with other optical systems), scalability and their ability to generate large optical delays with very fine resolution [4–8]. Fig. 1 shows a high-level schematic of a beam steering system with an OTTD engine and phased antenna array (PAA). The input radio frequency (RF) signal is first converted into an optical signal with a Mach–Zehnder modulator. This optical signal is first split into several signals by means of a power splitter. These optical signals are then delayed in the OTTD engine to achieve the desired delay outputs. The optical signals are finally converted back into RF signals through high-speed photodetectors (PDs) to excite the RF array. Note that the output optical signals are not generally equal in power because of various aberrations (e.g. spherical aberrations, astigmatism, coma etc.), and the different optical path lengths needed to achieve various delays. Obviously, the corresponding losses owing to misalignments, absorption, scattering etc., are different for each delay in the optical system. In Fig. 1, each of the four two-element sub-arrays of the antenna array use 3 dB couplers to ensure that both of the antennas in each sub-array are in phase and the power amplitude is the same. In any RF array, each antenna is influenced by the neighbouring antenna elements through mutual coupling. The main parameters needed to design/build a steerable array (with TTD) are the number of antenna elements, spacing of these elements as well as magnitude and time delay of each excitation. Therefore to generate a beam in the θ_m direction from broadside, the delays between adjacent elements should be Δt_{min}. Assuming the inter-element spacing is d and c is the speed of light in free space

$$\Delta t_{min} = \frac{d}{c} \sin \theta_m \tag{1}$$

Theoretically, these time delays are frequency independent; however, depending on their implementation, this is not always the case. This frequency independence can be achieved within a large frequency range if the delays are first generated in the optical domain. Furthermore, larger delays can be more efficiently implemented in the optical domain. As expected, as the steering angle becomes larger, the Δt_{min} becomes larger as well. Note that Δt_{min} is zero for $\theta = 0^{\circ}$ and equal to d/c for $\theta = 90^{\circ}$. Although the time delays can be very weakly dependent on frequency when implemented, the RF array is frequency dependent, especially the mutual coupling between the individual elements. This frequency dependence, as demonstrated here, has a deleterious effect on the performance of the array system and should be carefully considered when designing TTD RF beam steering systems.

In this paper, we present simulated and measured (RF array) results of a low-cost wideband antenna array (2–18 GHz) beam steering system integrated with a quadratic White cell OTTD engine. The optical delays are obtained by modelling the OTTD engine in a commercial software package (OSLO). The measured results for the RF array (scattering matrix and single-element radiation pattern) are combined with the simulated optical delays to steer the beam of the RF antenna array. We will analyse and discuss the effect of optical losses and mutual coupling between array elements in the RF beam steering, sidelobe levels and half-power beam width (HPBW). In Section 2,

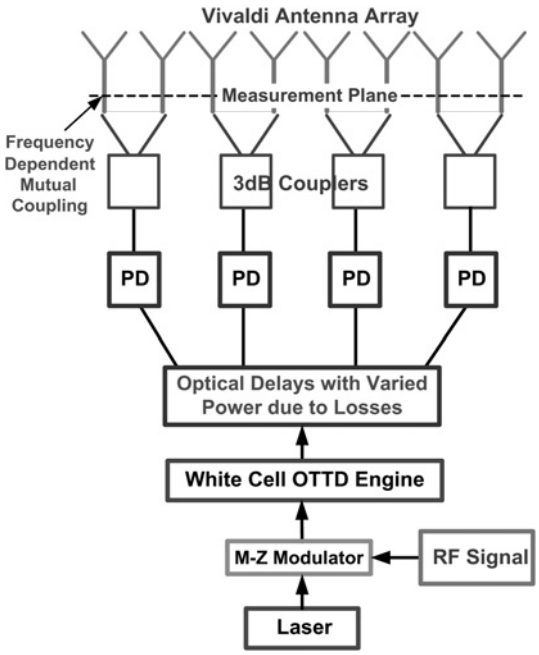

Fig. 1 *Schematic representation of RF array beam steering with OTTD engine*

we will briefly discuss some of the key components of the White cell OTTD engine. Section 3 is dedicated to the RF antenna array modelling as well as a discussion of beam steering using measured data of the Vivaldi antenna array and simulated optical/RF delays and losses in the White cell TTD. The paper ends with a summary and conclusions in Section 4.

2 White cell for beam steering

To demonstrate TTD beam steering, we need to create multiple time-delayed RF signals simultaneously and integrate the delays with a suitable wideband antenna array. Owing to the availability of only four PDs in our laboratory, we were constrained to a four-element RF array. We chose one of the simplest White cell TTD, referred to as a quadratic cell, to generate the delays for such a small antenna array.

Once the appropriate optical delays are generated, we need an array of PDs at the output of the OTTD engine to obtain the RF-delayed signals to feed the antenna array elements. Unfortunately, currently there are no commercially available arrays of high-speed PDs. The high-speed individual PDs available to us have an active area of 10 μm. Therefore the four outputs (25 μm) from the quadratic cell need to be de-magnified, relayed and separated to align with the appropriate bulky PDs while maintaining the beam size (1:1 imaging). Apart from the possible loss caused by beam aberration, reflection/transmission of optical surfaces, divergence and misalignment errors, there are additional losses in a system with multiple input beams because of beam separation at both the input and the output unit of the OTTD engine before they are linked to the array. In this paper we will show, as an example, how only one type of optical loss can affect the overall system performance significantly. The aberration loss calculation of this particular quadratic cell with and without a lens train (LT) (in its longer arm) has been reported in our previous publication (see Fig. 2) [9]. In this quadratic White cell,

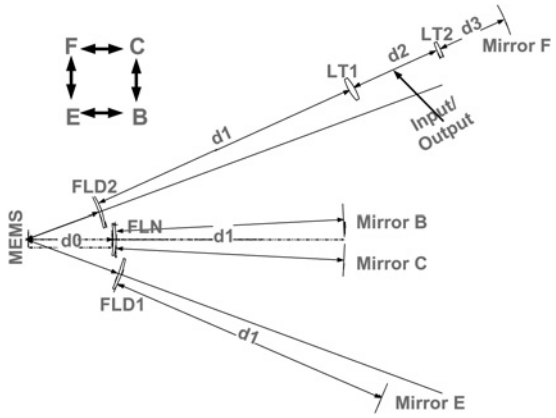

Fig. 2 *Layout of quadratic White cell and its connectivity diagram with LT for longer delays*

Table 1 Delay losses with and without LT along the long arm

Visiting arm	Delay, ps	Loss with LT, dB	Loss without LT, dB
null (B&C)	0	6.726	6.726
E once	25	6.712	6.712
E twice	50	6.835	6.835
F once	75	10.21	6.973
E once + *F* once	100	10.33	6.973
E twice + *F* once	125	12.03	7.007
F twice	150	14.34	6.977
E once + *F* twice	175	15.0	7.007
E twice + *F* twice	200	16.04	7.11
F thrice	225	18.88	6.976
E once + *F* thrice	250	20.82	7.007

arm *E* is to create short delay (e.g. 25 ps), whereas arm *F* is to create longer delay (e.g. 75 ps). The optical path length covered in arm *E* is in free space without any additional lenses other than the field lens. However, the optical path length covered in *F* requires two additional lenses, referred to as LT, to create longer delays while keeping the optical beam focused. The additional optical elements cause optical aberration loss, misalignment loss and additional Fresnel losses. In this paper, we will consider aberration loss as an example to show how any optical loss can affect the efficiency of an antenna array with OTTD. Table 1 shows the losses for each delay after six bounces (needed to create required number of delays) owing to aberrations, namely, astigmatism and spherical aberrations. The aberration loss using commercial optics is about 6.7 dB in the null cell. The longer arm, if it includes an LT, has about 3.5 dB more loss for delays of 75 ps than the arm without the lens train. Table 1 also shows that if we do not use any lens train, the loss per delay stays constant for short or long delays. Note that this loss calculation does not include misalignment errors or Fresnel loss.

3 Wideband antenna array

3.1 Mickey mouse Vivaldi antenna array measurement

The Vivaldi antenna is a special kind of tapered-slot antenna [10] (TSA) usually with an exponential flare. Besides being

efficient and lightweight, the more attractive features of TSAs are that they can work over a large-frequency bandwidth, produce a symmetrical end-fire beam with appreciable gain and low sidelobes [11] and high directivity [12]. The Vivaldis we used to build the array are called 'Mickey Mouse' Vivaldis [13]. By extending the exponential flare into a large circular arc instead of abruptly truncating them, these antennas prevent the pulse from ringing back and forth within the aperture. These antennas were constructed with a Duroid RT6002 substrate and have dimensions of 228.6 mm × 304.8 mm (see Fig. 3). The slot line width of the four original Vivaldi antennas designed for a previous research effort was only 2 mil [14]; this kind of precision was hard to match for commercial fabrication. Unfortunately, only one of those old antennas was working properly. All four newly fabricated antennas had a slot line width of ~5 mil and higher.

An array was built with a sub-array [15] architecture (as described in Fig. 4) using five antennas (*N*1, *N*2, *N*3, *N4* and *O4*) that were properly working and three antennas (*O*1, *O*2 and *O*3) that were not. The array consisted of a two-element sub-array with spacing of 2.2 cm between the elements and a spacing of 5.2 cm between the adjacent sub-arrays (see Fig. 4). As is well known, mutual coupling modifies the input impedance of each element and can also affect the element radiation pattern. The first step is to therefore measure the scattering matrix [$\boldsymbol{S}$] for the array. Using a two-port network analyser, we generated this matrix by making several two-port scattering parameter measurements. This set of two-port measurements was then used to generate the entire scattering matrix for a four-element array consisting of two-element sub-arrays under the assumption that the mutual coupling between nearest-neighbour sub-arrays is dominant. As shown in Fig. 4, a number of measurements were done with combinations of Configuration 1 (*C*1) with eight elements and Configuration 2 (*C*2) with all new four elements. As mentioned before, the letters *N* and *O* represent the new and old antennas, respectively. Configuration 1 (*C*1) was used to generate scattering matrix elements for the inner antenna elements (away from the edges of the array), whereas Configuration 2 (*C*2) was used to generate scattering matrix elements for the outer (edge) antenna elements.

The term *Near* and *Far* defines the interaction between the two elements of a sub-array and the elements that belong to different sub-arrays, respectively. This near/far scheme is used to calculate the coupling (or scattering) matrix from the measured data to simulate a synthetic array with eight antenna elements (four sub-arrays of two antennas each). Following the traditional synthetic array mechanism, whenever we performed a one-port measurement on a particular antenna ($\boldsymbol{S}_{ii}$), it had zero attenuation and the

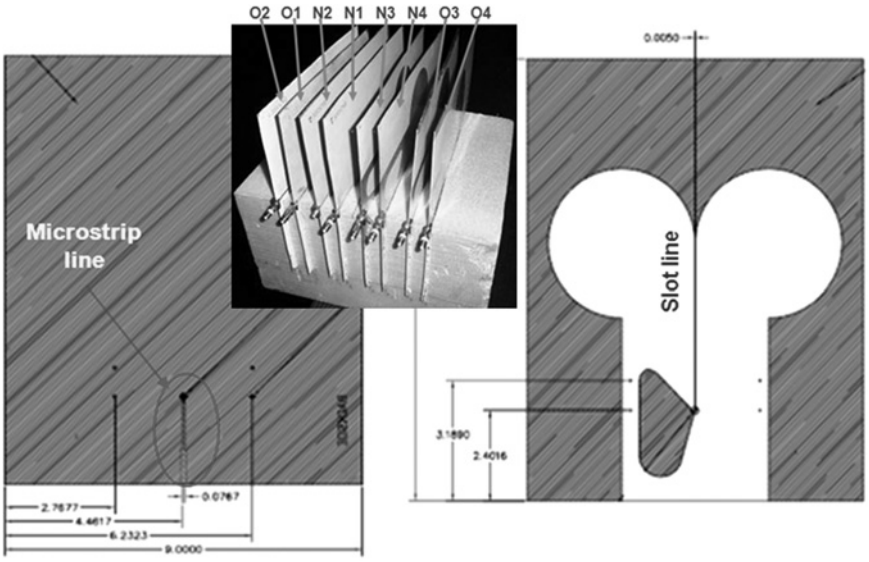

Fig. 3 *CAD diagram of the Vivaldi antenna*
Inset shows the actual Vivaldi array

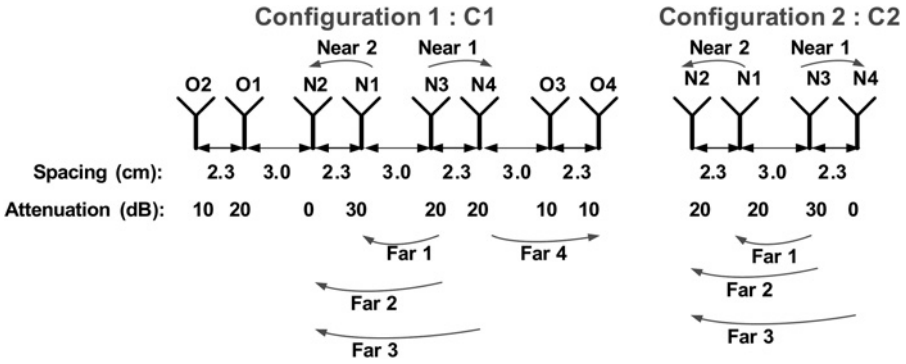

Fig. 4 *Actual implementation of Vivaldi antenna array measured data to simulate coupling matrix*

doi: 10.1049/iet-map.2010.0251

remaining antennas were terminated with attenuators to minimise unwanted reflections from them. Now, if element $N1$ receives complex signal b_j from element $N2$ excited by a signal a_i, then the scattering parameter $\boldsymbol{S_{ji}}$ can be defined as [16, 17]

$$\boldsymbol{S_{ji}} = \frac{b_j}{a_i}\bigg|_{a_k=0,\, k\neq i} \tag{2}$$

Fig. 5 shows the $\boldsymbol{S}_{ii}$ parameters of all the five Vivaldi antennas both in isolation and when they were embedded in the configuration described in Fig. 4. The results show (see Fig. 5*a*) that the $\boldsymbol{S}_{ii}$ parameters of all the new Vivaldis ($N1$, $N2$, $N3$ and $N4$) are compatible with the only old functioning antenna ($O4$). The old antenna only shows better performance at the lower frequencies. However, all the antennas satisfy the typical $\boldsymbol{S}_{ii}$ value of less than −10 dB in the frequency range of 4–14 GHz. Also, when the individual radiation patterns were measured, all the antennas show broad E-plane pattern in the frequency range of 4–18 GHz. All the antennas show more directional H-plane pattern in the frequency range of 4–18 GHz. However, as expected, the beam width is smaller at 18 GHz compared with the lower frequencies such as 4 and 5 GHz.

Fig. 6 shows three $\boldsymbol{S}_{ij}$ parameters for the array. Keeping in mind that the larger the separation between the elements the weaker the mutual coupling becomes – the curves shown in Fig. 6 are the dominant non-diagonal terms in the scattering matrix. That is why the mutual coupling decreases as the frequencies increases. Finally, if we compare the $\boldsymbol{S}_{ii}$ scattering matrix elements for the uncoupled and coupled cases (in Figs. 5*a* and *b*, respectively), it is obvious that the input impedance of the antennas degrade in the frequency ranges of 1–5 GHz and 10–12 GHz. Although not shown here, the strong coupling also deteriorates the radiation patterns of the individual antenna elements at the lower frequencies (1–5 GHz). Therefore the Vivaldi antenna array implemented here is most efficient in the frequency range of 5–10 GHz. The mutual coupling at the lower frequencies can be decreased by the alternative design of the Vivaldi element; however, it will not be considered here [18, 19].

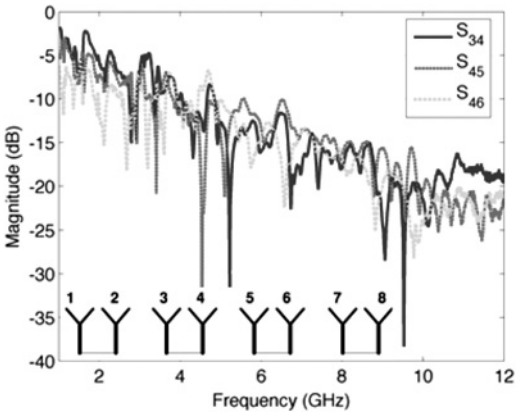

Fig. 6 *Mutual coupling as a function of frequency*

Before the discussion of our results are presented, it is important to note that traditionally two methods are used to generate array patterns, namely, 'isolated element pattern and active element pattern' [20]. In the isolated element pattern approach, the pattern of a single isolated antenna element is used in conjunction with the array factor where all the coupling effects in the total array pattern are accounted for in the scattering matrix. In the active element pattern approach, all the coupling effects are accounted for through the active element patterns themselves. In this paper, the former approach is used. This approach (isolated element pattern) is accurate for frequencies above 4 or 5 GHz where the mutual coupling is weaker and does not have much of an impact on the radiation pattern of the antenna elements.

3.2 Effects of mutual coupling and optical aberration loss on the array

Mutual coupling of the antenna elements in an array can substantially affect the main beam width, sidelobe levels and even the main beam levels. It is important to note that we define mutual coupling as the combination of inter-element coupling and antenna input impedance mismatch. Fig. 6 shows the mutual coupling elements of the array. As expected, the magnitudes of the mutual coupling elements

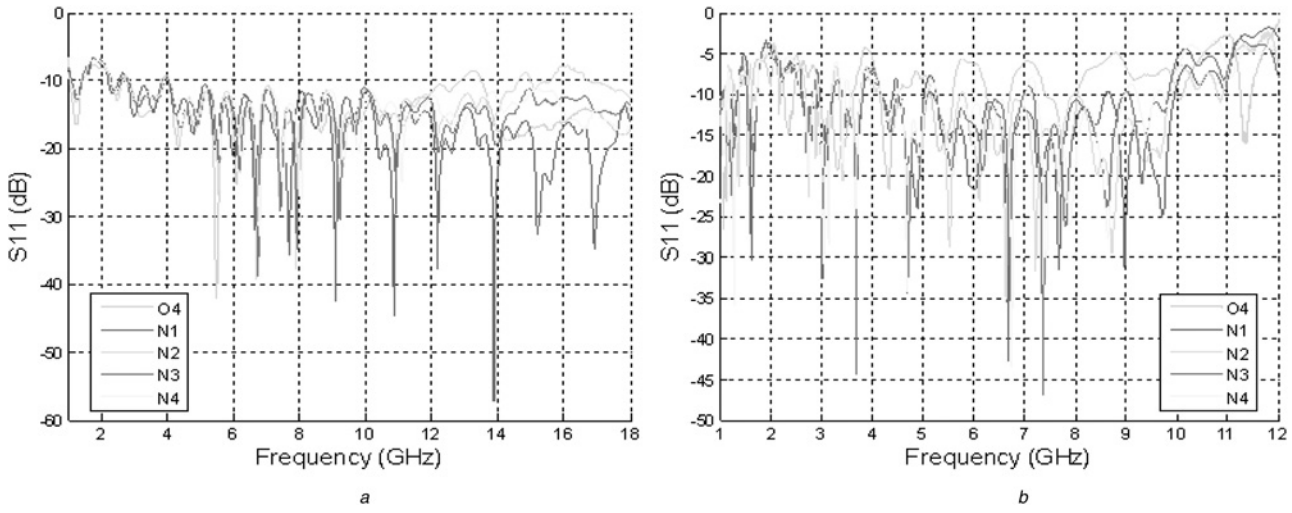

Fig. 5 *S-parameter of all five Vivaldi antennas*

a Isolated
b Embedded

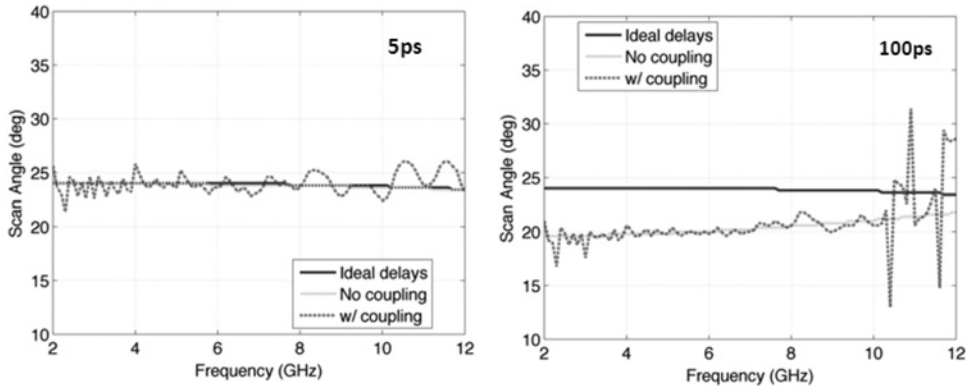

Fig. 7 *Mutual coupling as a function of scan angle and frequency with $\Delta t = 5$ ps and $\Delta t = 100$ ps*

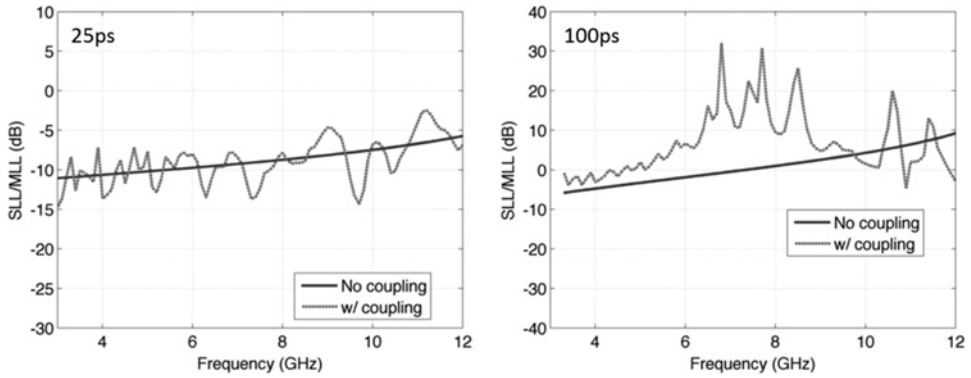

Fig. 8 *Mutual coupling as a function of sidelobe/main beam fraction and frequency with $\Delta t = 25$ ps and $\Delta t = 100$ ps*

decrease with frequency. In our case, however, we have a significant increase in the S_{11} level for all Vivaldi antennas over 10 GHz (we go from −10 to −5 dB). Therefore the error we are observing at high frequencies can be attributed solely to antenna input mismatch.

Running a parametric study on the sub-array, we also find out that the mutual coupling significantly increases the beam-pointing error at low frequencies. As we can see in Fig. 7, this effect is more pronounced for larger minimum time delay (Δt). The error is only about 2° for the 5 ps, whereas for 100 ps that increases to 5°. Also, antenna impedance mismatch causes substantial beam-pointing error at high frequencies (greater than 10 GHz).

Fig. 8 shows the graphs of the ratio of sidelobe level (SLL) to the main beam level as a function of frequency. The curve with coupling shows that the mutual coupling makes the first SLL higher over the whole frequency range, although at certain frequencies, the SLL is lower. Comparing the two cases of minimum time delay, we can conclude that as the minimum delay step increases, the mutual coupling drives the SLL to dominate the main beam level. Also, inter-element coupling generally increases the SLL at low frequencies, but has minimal effect at frequencies above 6 GHz. However, at those higher frequencies, antenna mismatch largely determines the SLL compared to inter-element coupling.

To see the effect of optical aberration loss on the array, we introduce the weighted optical loss (owing to optical aberrations in the White cell) from Table 1 for a quadratic cell with an LT to an isotropic sub-array to study the effect of optical aberration loss on the array. The weighted optical loss, actual and ideal delays of the array beam

Table 2 Sub-array excitation characteristics with optical loss at 7 GHz and Δt = 25 ps

actual delay, ps	225	150	75	0
ideal delay, ps	219.762	146.508	73.254	0
phase, deg	−153	−151.65	−152.15	−150.8
magnitude	0.11376	0.19187	0.30867	0.461

characteristics are tabulated in Table 2. As shown in Fig. 9, the smaller Δt (25 ps or smaller) increases the SLL almost to the level of the main beam. However, larger Δt (75 ps) either has no effect or surprisingly compensates for the errors because of quantisation and actually decreases the SLL. Even though, mutual coupling had no effect on the main beam HPBW, there was a small increase in the HPBW owing to optical aberration loss. However, this tendency was observed only for the small Δt, for example, 25 ps or smaller.

Studying the combined effects of both mutual coupling and optical aberration loss on the array performance, we see that performance degradation was dominated by the mutual coupling effect. Mutual coupling causes the substantial oscillations in SLL over the entire band (see Fig. 10). Comparing Fig. 10 with Fig. 8, we observe that at 25 ps, the shape of the SLL oscillations is similar, but the oscillations in Fig. 10 are shifted up by 2 dB with respect to those in Fig. 8. Comparing Fig. 10 with Fig. 8, this upward shift is simply because of the effect of the optical aberration loss. In the case of 75 ps, the SLL oscillations are also caused by mutual coupling effects, but are shifted downwards by 2 dB, since optical aberration loss

doi: 10.1049/iet-map.2010.0251

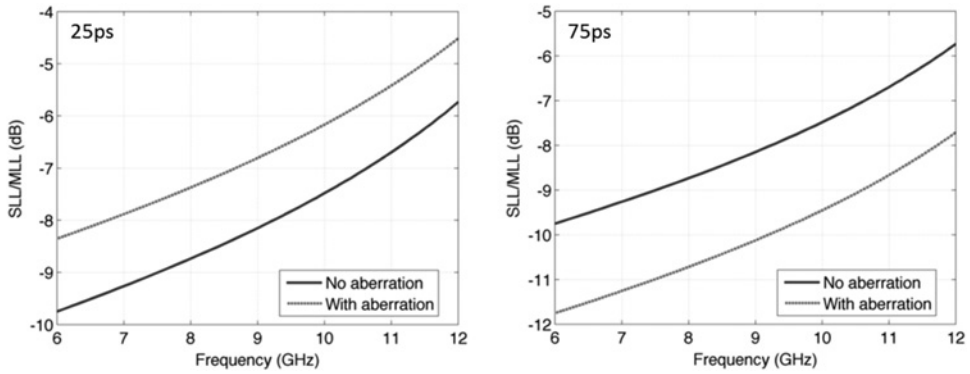

Fig. 9 *Optical loss as a function of sidelobe/main beam ratio and frequency for $\Delta t = 25$ ps and $\Delta t = 75$ ps*

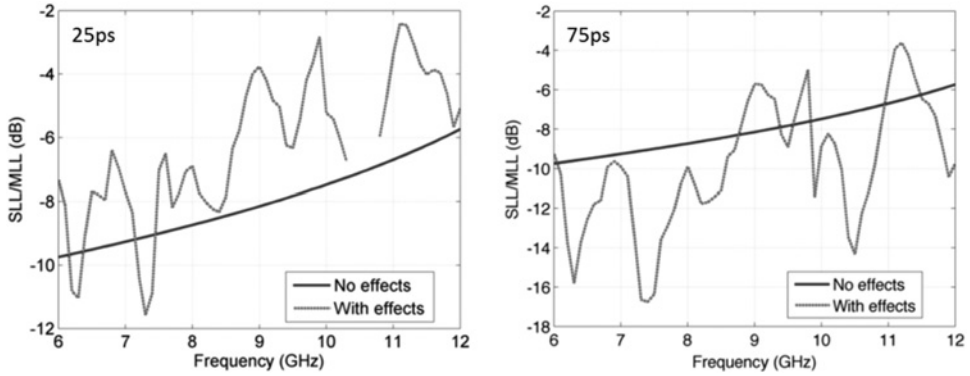

Fig. 10 *Combined effect of mutual coupling and optical loss on SLL for $\Delta t = 25$ ps and $\Delta t = 75$ ps*

suppresses the sidelobes by about 2 dB (see Fig. 9). The discontinuity in the SLL with combined effects for 25 ps is because of the absence of a well-defined first sidelobe.

Table 3 quantifies the main beam level degradation owing to scanning, mutual coupling and optical aberration loss. For 25 ps at broadside, the main beam level with optical loss relative to the level with mutual coupling is almost 5 dB lower. When the array is scanned to 25°, the case with optical loss is 10 dB lower than the case with mutual coupling. When the two effects are combined, the loss at broadside, as expected, is the sum of the losses owing to the separate effects. However, when the array is scanned to 25°, the loss owing to the combined effects is not the sum of the losses owing to the separate effects. That is, the loss owing to the combined effects is a non-linear function of loss owing to mutual coupling and loss owing to optical aberration.

Table 3 Array factor loss comparison at 7 GHz and $\Delta t = 25$ ps

Effect	Scan angle, deg	Array factor, dB
none	0	0
	25	−1.99
optical loss	0	−6.73
	25	−13.38
mutual coupling	0	−2.09
	25	−3.48
mutual coupling and optical loss	0	−8.82
	25	−14.21

Finally, for completeness we present in Table 4 a comparison table for our work with other's in this area of optical TTD. As we showed in this paper, the performance of the Vivaldi antennas is superb as individual wideband antennas. However, as in any antenna array, the performance deteriorates when they are embedded in an array mainly because of mutual coupling and excitation of grating lobes. Our antennas still show wideband performance from 4 to 10 GHz.

Table 4 Comparison of the optical loss and antenna bandwidth of optical TTD systems

Delay media	Min/max delay, ps	Delay step, ps	Optical loss/delay, dB	Actual antenna bandwidth, GHz
optical waveguide [3]	11.8/177	11.8	2.8	–
hybrid electronic and fibre optic [21]	57/1824	57	9.0	0.2–2.5
arrayed waveguide grating [22]	473/1073	40	6.8	–
fibre optic (fbg) [1]	−25/25	25	–	–
free-space (proposed system)	25/2000	25	6.726	4–10

4 Conclusions

In this paper, we have demonstrated an inexpensive and practical approach to construct a four-element sub-array wideband array for beam steering. The array shows wideband performance in the frequency range of 6–11 GHz with a scanning capability of $\pm 50^{\circ}$. A complication is that the four delays do not have the same magnitude because they are generated through different optical paths with different losses. The effect of this non-uniform excitation on the array is not insignificant. As an additional complication, although the OTTD signals are independent of frequency, mutual coupling is frequency dependent, and therefore the array performance is still frequency dependent, including the beam direction, sidelobe levels and HPWB. To obtain truly frequency-independent beam steering, it is therefore necessary to develop algorithms that can be applied to the RF-OTTD signals to compensate for the frequency-dependent mutual coupling.

5 References

1 Shin, J.-D., Bae, D.-H., Kim, B.-G.: 'Optical true time delay feeder for phased array antennas using Bragg grating and metal-film reflectors', *Microw. Opt. Technol. Lett.*, 2005, **45**, pp. 122–124

2 Barmenkov, Y.O., Cruz, J.L., Díez, A., Andrés, M.V.: 'Electrically tunable photonic true-time-delay line', *Opt. Express*, 2010, **18**, pp. 17859–17864

3 Howley, B., Wang, X., Chen, M., Chen, R.T.: 'Reconfigurable delay time polymer planar lightwave circuit for an X-band phased array antenna demonstration', *J. Lightwave Technol.*, 2007, **25**, pp. 883–890

4 Mital, R., Warnky, C.M., Anderson, B.L.: 'Design and demonstration of an optical true-time-delay device based on an Octic-style white cell', *IEEE J. Lightwave Technol.*, 2006, **24**, pp. 982–990

5 Warnky, C.M., Mital, R., Anderson, B.L.: 'Demonstration of Quartic cell, a free-space true-time-delay device based on White cell', *J. Lightwave Technol.*, 2006, **24**, pp. 3849–3855

6 Anderson, B.L., Rabb, D.J., Warnky, C.M., Abou-Galala, F.: 'Binary optical true-time delay based on the white cell: design and demonstration', *J. Lightwave Technol.*, 2006, **24**, pp. 1886–1895

7 Anderson, B.L., Collins, S.A., Mital, R., Nahar, N.K., Stone, B.R.: 'The 'Octic' White cell true-time delay device''. GOMAC Conf., April 2003

8 Higgins, R., Nahar, N.K., Anderson, B.L.: 'Design and demonstration of a switching engine for a binary true-time-delay device that uses a White cell', *Appl. Opt.*, 2003, **42**, pp. 4747–4757

9 Nahar, N.K., Rojas, R.G.: 'Low-loss polynomial White cell optical true-time delay engine for wideband radio frequency array beam steering', *J. Appl. Opt.*, 2009, **48**, pp. 3669–3676

10 Yang, L., Domier, C.W., Luhmann, N.C.: 'Ka-band E-plane beam steering/shaping phased array system using antipodal elliptically-tapered slot antenna', *Int. J. Infrared Millim. Waves*, 2007, **28**, pp. 283–289

11 Wang, H.Y., Mirshekar-Syahkal, D., Dilworth, I.J.: 'Rigorous analysis of tapered slot antennas on dielectric substrates'. IEE 10th Int. Conf. on Antennas and Propagation, April 1997

12 Janaswamy, R., Schaubert, D.H.: 'Analysis of a tapered slot antenna', *IEEE Trans. Antennas Propag.*, 1987, **AP-35**, pp. 1058–1065

13 Adams, J.C., Gregokch, W., Capots, L., Liccardo, D.: 'Ultra-wideband for navigation and communications', *IEEE*, 2001, **2**, pp. 785–791

14 Lai, A.K.Y., Sinopoli, A.L., Burnside, W.D.: 'A novel antenna for ultra-wide-band applications', *IEEE Trans. Antenna Propag.*, 1992, **40**, pp. 755–760

15 Mailloux, R.J.: 'Subarray technology for large scanning arrays'. Second European Conf. on Antennas and Propagation (EuCAP, 2007), Edinburgh, UK, 2007

16 Chen, S., Iwata, R.: 'Mutual coupling effects in microstrip patch phased array antenna'. Antennas and Propagation Society Int. Symp., IEEE, June 1998, vol. 2, pp. 1028–1031

17 Sadat, S., Chobadi, C., Nourinia, J.: 'Mutual coupling compensation in small phased array antennas'. Antennas and Propagation Society Int. Symp., 2004. IEEE, June 2004, vol. 4, pp. 4128–4131

18 Langley, J.D.S., Hall, P.S., Newham, P.: 'Balanced antipodal Vivaldi antenna for wide bandwidth phased arrays'. IEE Proc. Microwaves Antennas Propag., 1996, vol. 143, pp. 97–102

19 Bourqui, J., Okoniewski, M., Fear, E.C.: 'Balanced antipodal Vivaldi antenna for breast cancer detection'. Second European Conf. on Antennas and Propagation (EuCAP 2007), Edinburgh, UK, 2007

20 Stutzman, W.L., Thiele, G.A.: 'Antenna Theory and Design' (John Wiley & Sons, New York, 1981)

21 Goutzoulis, A.P., Zomp, J.M.: 'Development and field demonstration of an eight-element receive wavelength-multiplexed true-time-delay steering system', *Appl. Opt.*, 1997, **36**, pp. 7315–7326

22 Yeniay, A., Gao, R.: 'True time delay photonic circuit based on perfluorpolymer waveguides', *IEEE Photonics Technol. Lett.*, 2010, **22**, pp. 1565–1567

doi: 10.1049/iet-map.2010.0251